Environmental Science: Atmospheres

ROYAL SOCIETY OF CHEMISTRY

PAPER

View Article Online
View Journal

Cite this: DOI: 10.1039/d5ea00122f

Measurements and model comparisons suggest that HONO is not an important source of OH radical concentrations below a rural forest canopy

Bode Hoover,[a] Emily Reidy,[b] Ian Spink,[a] Amanda Hamachek,[b] Brandon Bottorff[b] and Philip S. Stevens *[ab]

The hydroxyl radical (OH) initiates the oxidation of volatile organic compounds (VOCs) in the atmosphere, leading to the production of ozone and secondary organic aerosols (SOA). While nitrous acid (HONO) can be an important OH source during the daytime, the mechanisms controlling HONO concentrations remain poorly understood, with unknown sources commonly reported. To improve our understanding of their sources and sinks, HONO and OH concentrations were measured below a forest canopy using a Laser-Photofragmentation/Laser-Induced Fluorescence instrument and were modeled using a zero-dimensional model based on the Master Chemical Mechanism. Heterogeneous conversion of NO_2 on ground surfaces dominated nighttime HONO production (95%) while the reaction between OH and NO was the dominant daytime source (77%). Deposition was a primary HONO removal process at night (99%) and during the day (64%) followed by photolysis (34%). Overall, the model was able to reproduce the HONO measurements, although it could not reproduce observed increases in HONO during individual rain events, which were likely due to elevated heterogeneous production. Measured concentrations of OH were similar to previous observations above the canopy at this site, suggesting that significant chemical oxidation was occurring in the canopy that could impact the concentration of oxygenated VOCs and SOA above the canopy. Ozonolysis of monoterpenes was a dominant source of radicals below the canopy, accounting for 70% of total radical initiation. Photolysis of HONO contributed approximately 1% to total radical initiation, suggesting that at this site HONO is not an important source of OH radicals beneath the canopy.

Received 26th September 2025
Accepted 9th March 2026

DOI: 10.1039/d5ea00122f

rsc.li/esatmospheres

Environmental significance

The hydroxyl (OH) radical is the dominant atmospheric oxidant, initiating the production of ground-level ozone and secondary organic aerosols (SOA). While photolysis of nitrous acid (HONO) can be a significant source of OH, the sources of HONO remain poorly understood. In contrast to several previous studies, measurements of HONO below a midlatitude forest canopy could be explained by known formation mechanisms. Though HONO did not contribute significantly to radical production at this site, the ozonolysis of biogenic volatile organic compounds was a dominant source of radicals, resulting in below canopy concentrations similar to that observed above the canopy. These results suggest that significant oxidation may be occurring in the canopy that could impact the concentration of SOA above the canopy.

1. Introduction

The hydroxyl radical (OH) is the primary daytime tropospheric oxidant which initiates the oxidation of volatile organic compounds (VOCs) that leads to the production of hydroperoxy radicals (HO_2) and organic peroxy radicals (RO_2). In the presence of nitrogen oxides ($NO_x = NO + NO_2$), these reactions can lead to the production of ozone and secondary organic aerosols in the atmosphere. Because of their central role in atmospheric chemistry, understanding the sources and sinks of the OH radical is important to accurately address current issues of air quality.

Atmospheric chemistry models have often overpredicted surface ozone levels above forested areas of the eastern United States.[1] Previous studies have found that stomatal uptake of ozone alone cannot account for the observed ozone fluxes below and within forest canopies where the missing flux correlates with terpene emissions and temperature.[2–4] Recent studies suggest that non-stomatal loss accounts for a significant fraction of ozone deposition, with in-canopy chemistry only accounting for a small fraction of total ozone fluxes,[5] and 1-D forest canopy modelling suggests that OH radical

[a]O'Neill School of Public and Environmental Affairs, Indiana University, Bloomington, IN, USA. E-mail: pstevens@iu.edu
[b]Department of Chemistry, Indiana University, Bloomington, IN, USA

concentrations at the surface are significantly lower than that above the forest.[6] However, the rapid ozonolysis of unaccounted for biogenic VOCs could lead to the production of OH radicals and secondary pollutants, including VOCs and SOA oxidized by both OH and ozone, which could impact the above canopy environment.[4,7–9] Unfortunately, there have been few below canopy measurements that describe the sources and sinks of radical species near the forest floor.

Several studies have recognized that the photolysis of nitrous acid (HONO) can be a dominant source of OH radicals.[10,11] However, the sources of HONO are not well understood, with direct emissions from combustion,[12] heterogeneous production on surfaces,[13] nitrate photolysis,[14] and soil emissions proposed to contribute to observed concentrations.[15] Elevated concentrations of HONO from surface sources could still be a significant source of OH radicals despite the reduced photolysis rates beneath the canopy.

In the gas phase, HONO is produced from the reaction of OH and NO (R1).[16] Photolysis is the dominant sink for atmospheric HONO during the day (R2) with the reaction with OH (R3) serving as a minor daytime sink.[17,18]

$$\mathrm{OH} + \mathrm{NO} \xrightarrow{\mathrm{M}} \mathrm{HONO} \quad \text{(R1)}$$

$$\mathrm{HONO} + h\nu \xrightarrow{\lambda < 400\mathrm{nm}} \mathrm{NO} + \mathrm{OH} \quad \text{(R2)}$$

$$\mathrm{HONO} + \mathrm{OH} \rightarrow \mathrm{NO_2} + \mathrm{H_2O} \quad \text{(R3)}$$

Models that are limited to gas-phase production and loss of HONO generally underpredict measured concentrations, sometimes by as much as an order of magnitude during the daytime, illustrating the significance of additional sources.[19–21]

The heterogeneous conversion of NO_2 on wet surfaces (R4) is the dominant heterogeneous pathway and can be photoenhanced.[22–25]

$$2\mathrm{NO_{2(g)}} + \mathrm{H_2O_{(ads)}} \xrightarrow{\text{surface}} \mathrm{HONO_{(ads)}} + \mathrm{H_{(aq)}}^{+} + \mathrm{NO_{3(aq)}}^{-} \quad \text{(R4)}$$

In some rural and remote areas, the NO_x concentrations are too low to account for elevated HONO concentrations,[19,26] leading to the proposal that the photolysis of surface nitric acid (HNO_3) and particulate nitrate (pNO_3^-) (R5) are significant contributors.[21,26–28]

$$\mathrm{HNO_{3(ads)}}, \mathrm{pNO_3}^{-} + \mathrm{H_2O_{(ads)}} + h\nu \xrightarrow{\lambda < 320\mathrm{nm}} \mathrm{HONO_{(g)}} + \mathrm{NO_{x(g)}} \quad \text{(R5)}$$

HONO can also be lost through both dry and wet surface deposition which is dependent on the surface characteristics, turbulence, and the boundary layer height.[29–31]

Soil microbial activity has also been proposed to be a significant source of HONO.[29] However, the influence of soil-derived HONO on atmospheric radical chemistry across forest environments remains poorly understood. Emissions from soil vary with factors such as moisture content, pH, organic matter, and microbial community composition, making the role of different soil types uncertain.[15,32–37] Laboratory experiments have shown that microbial processes during nitrification and denitrification can generate HONO, as ammonium and nitrate are converted to nitrite.[32,36] Fertilized agricultural soils, in particular, have been observed to emit substantial amounts of HONO.[38] Although the exact mechanisms of HONO production and release in soils are still under investigation, a range of soil microbes, including ammonia-oxidizing bacteria (AOB), ammonia-oxidizing archaea (AOA), methane-oxidizing bacteria, heterotrophic nitrifiers, and fungi, are thought to contribute to the production of HONO. One proposed pathway involves the emission of hydroxylamine (NH_2OH) by nitrifying bacteria, which then reacts heterogeneously with water vapor to form HONO.[33]

Recent modeling studies have highlighted the potential importance of soil HONO emissions for below-canopy atmospheric chemistry. In agricultural regions, model results suggest that emissions of HONO from fertilized soil can increase OH radical production by 41% and consequently affect the formation of secondary pollutants.[39,40] This has sparked growing interest in quantifying soil HONO fluxes across different ecosystems, particularly in forest environments where the coupling between surface emissions and canopy-scale radical budgets remains poorly constrained.

The goals of this study were to (1) examine temporal trends of HONO and OH radical concentrations below a forest canopy, (2) evaluate the contribution of surface interactions and emissions to HONO formation and loss, and (3) quantify the role of HONO and other sources to OH radical production beneath the canopy. To this end, measurements of HONO and OH radical concentrations were conducted below the forest canopy during the Michigan Observations of the Below Canopy ATmosphere (MOBCAT) field campaign. These observations were compared with predictions from a zero-dimensional box model constrained by measured trace gas concentrations and meteorological conditions. The model included a pH- and relative humidity-dependent parameterization of NO_2 and HONO surface uptake to assess the impact of surface interactions on below-canopy HONO and OH photochemistry.

2. Methods

2.1 Measurement site

The MOBCAT field campaign was conducted at the Program for Research on Oxidants: PHotochemistry, Emissions, and Transport (PROPHET) site at the University of Michigan Biological Station (UMBS) (45°30′N, 84°42′W) from July 25 to August 12, 2022. The PROPHET site is in a mixed deciduous and coniferous forested comprised of maple, aspen, oak, and pine trees near the northern tip of the rural Michigan Lower Peninsula with a canopy height between 21 m and 22 m.[41–43] The PROPHET research site is 3.5 km west of the UMBS with the nearest town of Pellston located about 5.5 km further west. The site has been described in detail elsewhere.[42,43] Measurements were taken on the south side of the PROPHET laboratory (Fig. S1).

The concentration of isoprene was measured by gas chromatography flame ionization detection (GC-FID) (Agilent 7890B) coupled with a thermal desorber (TD) (Markes International Unity Series 2). The concentration of NO_2 was measured

by a Thermo NO_x Analyzer (Model 42C) and ozone was detected by a Teledyne Instruments photometric O_3 analyzer (Model 400E). Relative humidity and temperature were monitored by a Vaisala HMP60 probe placed near the sampling inlet. The photolysis rate of NO_2 (J_{NO_2}) was measured using a 2π actinic filter radiometer (Meteorologie Consult GmbH/METCON, Germany). Further details for supporting measurements are provided in the SI (Table S1). Because measurements of NO were below the detection limit of the instrument, mixing ratios of NO were constrained in model runs based on the average below canopy measurements of NO made at this site in 2016.[44] These values are similar to that calculated using the photostationary state during the day (Fig. S2). The diurnal averaged values from 2016 were used instead of the photostationary state calculated NO in the average model as the photostationary state concentrations of NO may be lower than the actual NO levels as a result of downward transport of NO from above the canopy.[45] However, to assess the impact of precipitation on the sources and sinks of HONO during individual days when rain was observed, photostationary state derived NO values were used to predict HONO concentrations as discussed in Section 4.2.

To determine the soil pH and its contribution to HONO production and loss, six soil samples were collected at a depth of 6 cm using a standard soil sampler ranging from 6 cm to 70 cm away from the detector (Fig. S3). Soil samples were frozen until the pH was tested by mixing each soil sample with an equal amount of water (50 : 50 ratio) and inserting a Mettler Toledo Five Easy Plus pH meter (FP20) directly into the mixture.[46]

2.2 Measurements of HONO and OH using laser photofragmentation-laser induced fluorescence

A laser photofragmentation-laser-induced fluorescence (LP-LIF) instrument, described in detail elsewhere,[47] was used to measure HONO and OH. Briefly, ambient air is sampled through a 0.64 mm diameter pinhole inlet located 45 cm above the bare soil and expanded into a low-pressure chamber at a pressure of approximately 200 Pa. A Spectra Physics Navigator II YHP40-355HM producing approximately 3–4 W of radiation at 355 nm and at a repetition rate of 10 kHz photolyzes HONO into OH and NO, and the OH fragment is detected by laser-induced fluorescence. Approximately 20–40 mW of radiation at 308 nm with a repetition rate of 10 kHz was generated by a tunable dye laser (Sirah Credo) that was powered by the second harmonic of a Spectra Physics Navigator II YHP40-532 Nd-YAG laser. The excitation and photofragmentation laser emissions were propagated to the sampling cell by 12 m fiber optic cables (excitation: ThorLabs FG200AEA; photofragmentation: OZ Optics custom fiber, NA = 0.22, core diameter = 1000 μm) and are spatially joined by a dichroic mirror before entering the detection cell. The laser pulses are temporally separated, with the 308 nm pulse entering the detection cell 100 ns after the 355 nm pulse.

OH radicals are excited and detected using the $A^2\Sigma^+ v' = 0 \leftarrow X^2\Pi v'' = 0$ transition near 308 nm. The OH fluorescence is detected using a microchannel plate photomultiplier tube (MCP-PMT) detector (Photek PMT 325), a cathode gating module (Photek GM10-50B), and an amplifier/discriminator (Advanced Research Instruments Corp F-100T).[8] To differentiate the OH fluorescence from any background signals such as laser scatter that extends into the gated detection window, the laser wavelength is modulated spectrally on- and off-resonance with the $Q_1(3)$ transition of OH near 308 nm. The OH fluorescence signal is obtained by subtracting the off resonant signal from the resonant signal. To ensure that the laser is tuned on and off from the OH transition, a reference cell is used where OH is produced by the thermal dissociation of water vapor. Ambient OH concentrations are measured when the 355 nm photofragmentation laser is blocked, allowing nearly simultaneous measurements of both HONO and OH concentrations.

The instrumental sensitivity to OH is determined by producing a known amount of OH through the photolysis of water vapor at 184.9 nm.[48] Calibrations performed intermittently throughout the campaign resulted in an OH detection limit of 5.9×10^5 cm^{-3} (2 h average, S/N = 2). While the LP/LIF instrument can measure potential interferences using C_3F_6 addition to scavenge ambient OH and measure any internally generated OH,[49,50] the technique was not used during MOBCAT to increase the HONO measurement frequency. Therefore, the OH measurements are considered an upper limit. The HONO photolysis efficiency was measured as described previously,[47] and a value of 0.41% was used to extract the HONO concentration from the measured concentration of the OH fragment. The HONO detection limit was approximately 14 ppt (2 h average, S/N = 2), with an overall calibration uncertainty of 35% (1σ).[47]

2.3 Modeling of HONO and OH concentrations

The diurnal averaged measurements of OH and HONO were modeled with the Framework for 0-Dimensional Atmospheric Modeling using the Master Chemical Mechanism (MCM Version 3.3.1) and includes a version of the updated Leuven Isoprene Mechanism (LIM1).[51–55] The zero-dimensional photochemical box model was constrained to the 1 hour average measured mixing ratios of trace species (O_3, NO, NO_2, and VOCs) and meteorological parameters (relative humidity and temperature) then processed through a 3-day spin-up cycle to generate unmeasured secondary oxidation products. The model was additionally constrained to the measured OH concentrations when modeling HONO and constrained to the measured HONO when modeling OH concentrations. Similar to previous studies, horizontal and vertical transport of HONO below the canopy was assumed to be negligible.[56,57]

Sesquiterpenes were not measured but included as β-caryophyllene in the model by estimating the total concentration using a temperature dependent proxy.[58] When speciated measurements of monoterpenes and oxygenated VOCs were not available, an average of previous measurements at this site was used to constrain the model.[44] Measurements of isoprene were similar in magnitude and diurnal trend to previous measurements, supporting the use of past measurements for other terpenes (Fig. S4).[44] The atmospheric lifetime was set to 1 hour

(k_{dil}), shortening the lifetime of unmeasured modeled oxidation products so that the modeled total OH reactivity was similar to previous measurements at this site (Fig. S5).[44,59]

Photolysis frequencies were estimated using a trigonometric parameterization based on the solar zenith angle.[55,60] Photolysis rate constants (*e.g.*, J_{HONO}) were scaled by J_{corr}, defined as the ratio of the measured J_{NO_2} to the J_{NO_2} predicted under ideal conditions by the (National Center for Atmospheric Research Tropospheric Ultraviolet and Visible) Radiation Model.[61] The model uncertainty is estimated to be approximately 30% (1σ).[55,62]

The HONO production and loss rates are determined by the following:

$$P_{known} = P_{OH+NO} + P_{ground} + P_{other} \quad (E1)$$

$$L_{known} = L_{photo} + L_{OH+HONO} + L_{HONO+ground} + L_{other} \quad (E2)$$

Here P_{known} and L_{known} are the sum of the known production and loss rates (ppb h^{-1}), respectively. A detailed discussion of all HONO sources and sinks included in the budget is provided in the SI (Text S1 and S2).[63–67] In the base model, only the homogeneous gas phase production of HONO through the reaction between OH and NO (E3) is considered along with the two loss rates of photolysis (E4) and reaction with OH (E5).

$$P_{OH+NO} = k_{OH+NO}[OH][NO] \quad (E3)$$

$$L_{photo} = J_{HONO}[HONO] \quad (E4)$$

$$L_{OH+HONO} = k_{OH+HONO}[OH][HONO] \quad (E5)$$

Heterogeneous chemistry involving surface interactions, including photoenhanced heterogeneous chemistry, was incorporated into the updated model using the parameterizations and mechanisms listed in Tables S2 and S3.[17,56,68–75]

The main production (E6) and loss (E7) mechanisms involving ground surface interactions are summarized by the equations below which are consistent with previously reported methods with the addition of meteorologically dependent uptake coefficients.[28,29,76]

$$P_{ground} = \frac{\gamma_{NO_2} \nu_{NO_2}}{8} \frac{S_{ground}}{V} \frac{RH}{50} [NO_2] \quad (E6)$$

$$L_{HONO+ground} = \frac{\gamma_{HONO} \nu_{HONO}}{8} \frac{S_{ground}}{V} \frac{RH}{20} [HONO] \quad (E7)$$

Here P_{ground} is the production rate of HONO through the heterogeneous interaction of NO_2 with ground surfaces (ppb h^{-1}) and $L_{HONO+ground}$ is the loss rate of HONO due to ground deposition (ppb h^{-1}), where $\frac{S_{ground}}{V}$ is the estimated surface-area-to-volume ratio for the ground surface based on the estimated boundary layer height (BLH) (Table S2).[29,77,78] The molecular velocity (v_i) for species i is represented by:

$$\nu_i = \sqrt{\frac{3RT}{M_i}} \quad (E8)$$

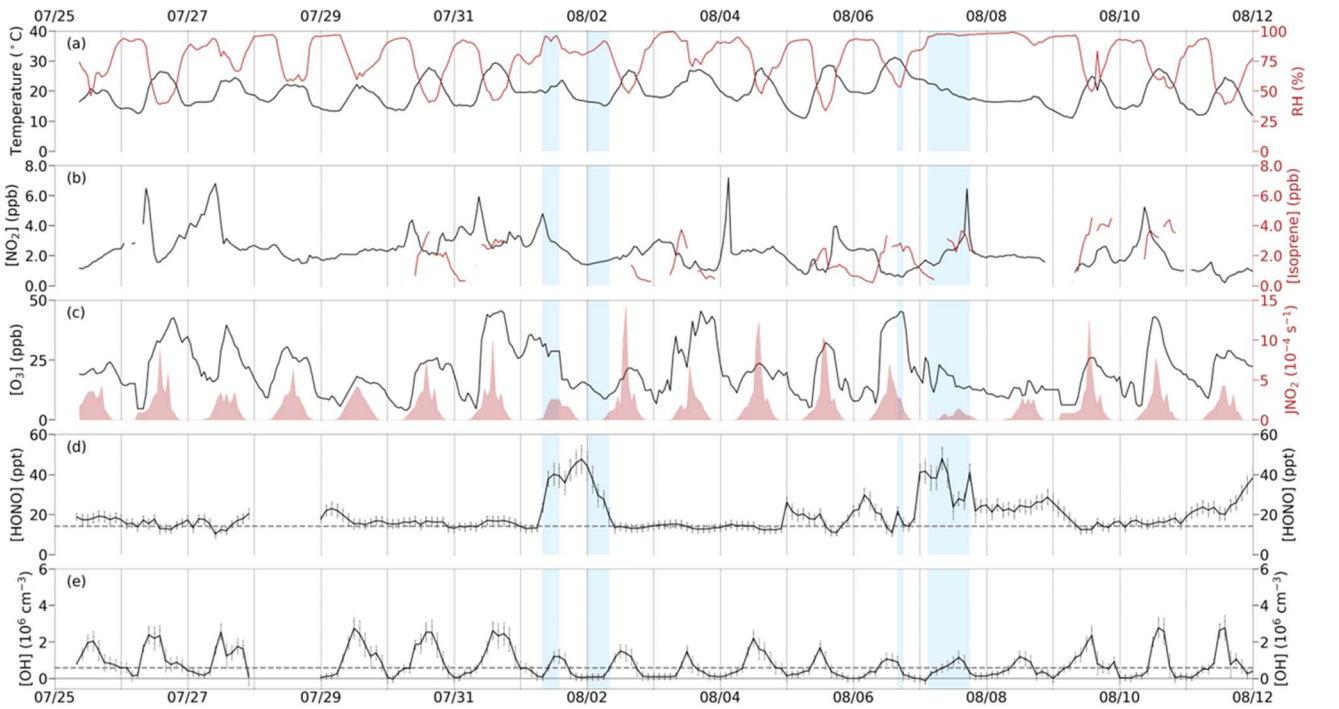

Fig. 1 Time series of measured meteorological (a) and chemical conditions (b–e) data collected during the MOBCAT field campaign from 25 July to 12 August 2022. Blue shaded regions represent rain periods. The error bars represent two standard deviations of the mean (d, e) and the gray dashed lines in (d) and (e) represent the average limit of detection (S/N = 2, 2 hours average) for HONO (14 ppt) and OH (5.9×10^5 cm^{-3}).

Here R is the ideal gas constant (8.314 J mol^{-1} K^{-1}), T is the temperature (K), and M_i is the molar mass of species i (g mol^{-1}, *e.g.* HONO, NO_2).

The uptake coefficient of NO_2 on the ground (γ_{NO_2}) has been empirically shown to be related to the relative humidity (RH) (E9).[56,68]

$$\gamma_{NO_2} = 5.5 \times 10^{-8} \times RH + 7.4 \times 10^{-7} \quad (E9)$$

The calculated values of approximately 10^{-6} used in this study were within the range of reported values.[29,56,68,79] The uptake coefficient of HONO on the ground (γ_{HONO}) was calculated based on best fit functions for compiled empirical studies of the dependence on pH and relative humidity on various surfaces (E10)–(E12).[70–72,80,81]

$$\gamma_{HONO} = \varphi_{pH} + \varphi_{RH} \quad (E10)$$

$$\varphi_{pH} = 3.604 \times 10^{-6}\ pH^2 - 4.21 \times 10^{-5}\ pH + 1.549 \times 10^{-4} \quad (E11)$$

$$\varphi_{RH} = 2.0 \times 10^{-4} \times RH^{-0.043} \quad (E12)$$

Here φ_{pH} is the pH dependence and φ_{RH} is the relative humidity dependence, respectively. The calculated NO_2 uptake coefficient is lower in magnitude and shows greater diurnal variability minimizing during the day (Fig. S6). Parameters included in the adjusted model are summarized in Table S2 and were in the range of previously reported values.[82]

3. Results

3.1 Meteorological and chemical conditions

The daily campaign meteorological conditions and important chemical species are provided in Fig. 1, with the diurnal averaged measurements in Fig. 2 and summary statistics of the field campaign measurements in Table S4. Periods when precipitation occurred are indicated by the blue shaded regions in Fig. 1. NO_2 mixing ratios averaged 2.25 ± 0.22 ppb and tended to decrease during the rain events. O_3 ranged from 4.1 to 45.5 ppb

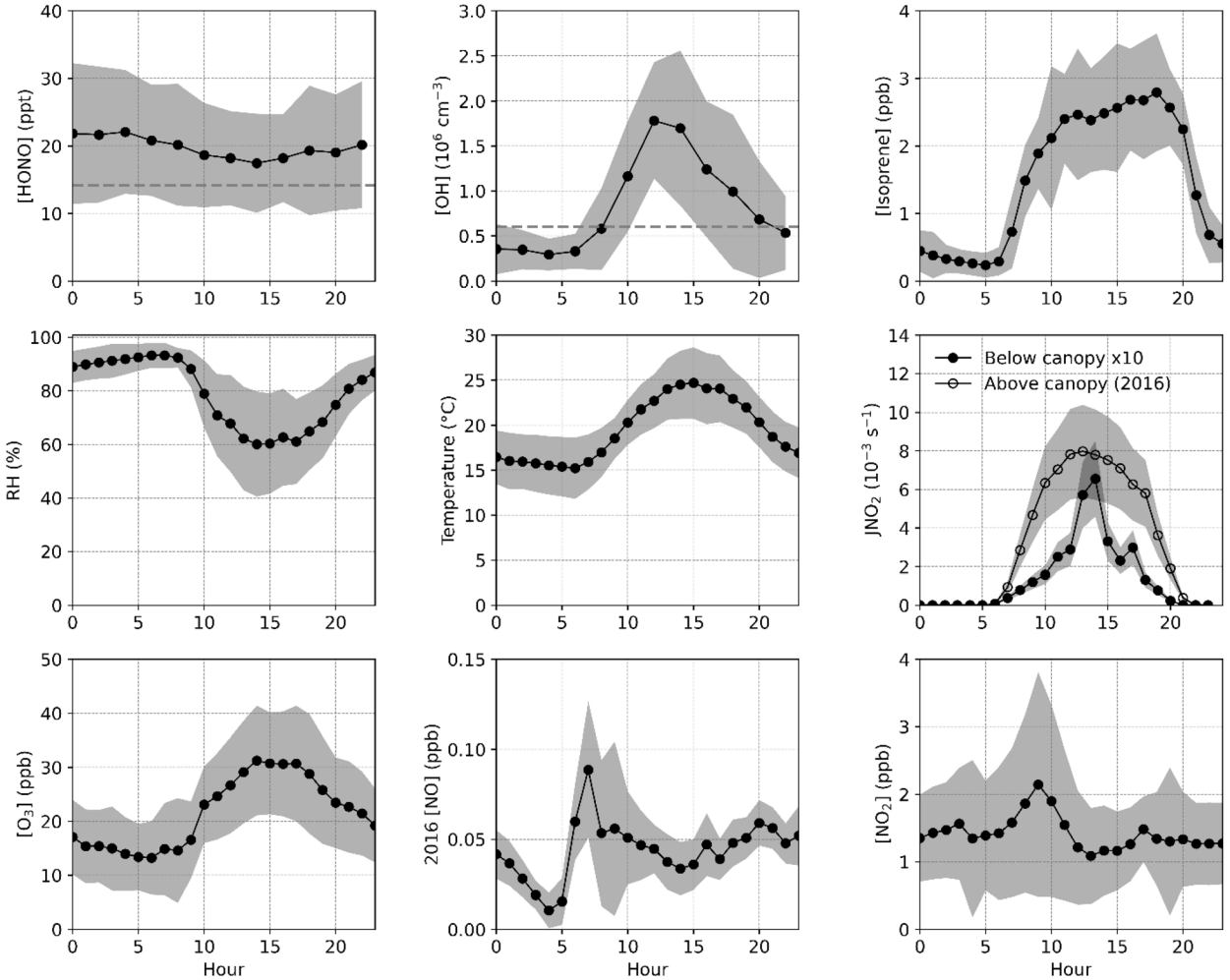

Fig. 2 Diurnal trends of below canopy measurements where shaded regions represent one standard deviation of variability. Dashed gray lines represent the average limits of detection for HONO and OH. Solid circles represent measurements during the MOBCAT 2022 field campaign while the open circles represent J_{NO_2} above canopy measurements from 2016.[44] Note the order of magnitude difference in scale between the J_{NO_2} above and below canopy.

with an average of 20.3 ± 2.1 ppb peaking around 13:00. The photolysis rates below the forest canopy were reduced to approximately 4% of the rates above the canopy (Fig. 2).[44] The NO_2 photolysis rate (J_{NO_2}) peaked around 13:00 with a maximum of 1.44×10^{-3} s^{-1} and an overall average of $(1.35 \pm 0.21)\times10^{-4}$ s^{-1}, which was lower during the rain events. Isoprene ranged from 0.5 ppb to 3.5 ppb with a consistent afternoon peak around 15:00. These measurements are similar in both magnitude and trends to previous campaigns conducted at the PROPHET site (Table S5).[26,83–85]

3.2 HONO measurements and model predictions

The average HONO mixing ratio during the campaign was 19.8 ± 6.9 ppt with a maximum of 51.9 ppt on August 7 at 08:00 (Fig. 1). HONO average mixing ratios were typically higher during nighttime and lowest during daytime ($p < 0.01$). Fig. 3 shows the campaign average measured and modeled HONO mixing ratios. When including only gas phase chemistry, the model overpredicts the measurements during the night and underestimates the daytime mixing ratio of HONO when constrained to the measured OH and the average below canopy measurements of NO from 2016 (Fig. 3). However, including heterogeneous chemistry involving surface production and loss of HONO improves the agreement of the model with the measured concentrations, although the model does underestimate the daytime mixing ratio by approximately 33% (Fig. 3). However, these results suggest that the model can reproduce the measured concentrations to within the combined uncertainties of the measurements (±35%) and an estimated model uncertainty range of ±30%.[47]

An analysis of the modeled HONO production and loss mechanisms under dry conditions reveals a strong diurnal dependence on both chemical and physical processes (Fig. 4). During nighttime (20:00–08:00), the shallow boundary layer enhances interactions between atmospheric NO_2 and ground surfaces, leading to significant heterogeneous conversion of NO_2 to HONO. This pathway accounted for approximately 95% of nighttime HONO production. By contrast, during daytime (08:00–20:00), the reaction of OH with NO dominates HONO formation, contributing around 77% of total production, with surface-mediated NO_2 conversion playing a secondary role (23%). Loss processes also follow a clear pattern: during the day, HONO is primarily removed through deposition (64%) and to a lesser extent *via* photolysis (34%). At night, deposition becomes the dominant sink, responsible for 99% of HONO loss. Reactions involving aerosol surfaces were negligible in comparison to ground surface interactions. Surface acidity may influence HONO partitioning between surfaces and the atmosphere, analogous to the pH-dependent volatilization of NH_3 previously observed at this site.[86] Unfortunately, soil pH measurements were only done on a single day, preventing a detailed analysis of whether temporal variations in surface acidity may have affected HONO emissions during the study period.

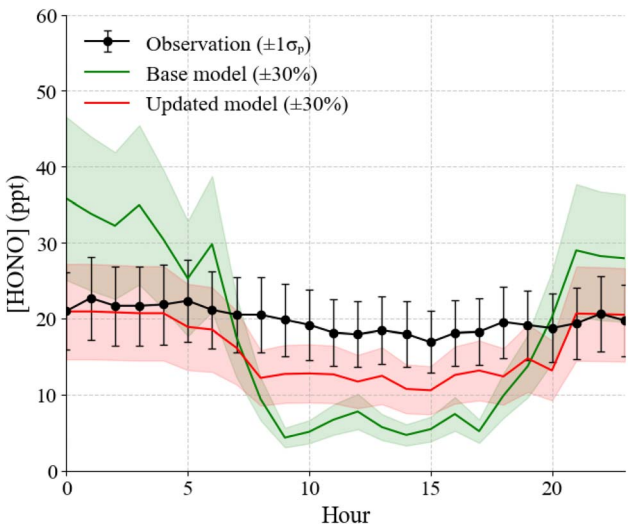

Fig. 3 Comparison between the measured HONO mixing ratios (black) and the predicted values resulting from the base model (green), and the updated model (red). Model results have an estimated 30% error while error bars for the measured HONO represent the measurement precision (±1σ_p) and do not include the calibration uncertainty (±35%, 1σ).

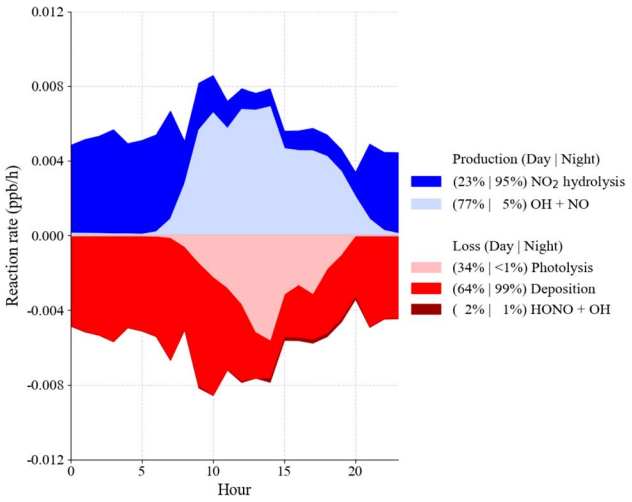

Fig. 4 HONO budget for the adjusted model with average daytime (08:00–20:00) and nighttime (20:00–08:00) contributions to total production (blue) and loss (red) during dry periods. Other production and loss mechanisms were negligible.

3.3 OH measurements and model predictions

The average OH concentration measured during the campaign was $(8.3 \pm 1.6)\times10^5$ cm^{-3}, with a maximum daytime value of $(3.0 \pm 0.2)\times10^6$ cm^{-3} observed on July 31, 2022 (Fig. 1). The average maximum OH concentration measured below the canopy of approximately 2.3×10^6 cm^{-3} is similar to that measured previously above the canopy at this site where no significant interference was observed (Fig. S7),[44,62] but larger than that predicted by a 1-D canopy model of this site.[6] Because interference testing was not conducted during this campaign,

these OH measurements should be considered an upper limit to the actual concentrations.

Fig. 5 shows the measured and modeled OH concentrations when the model is constrained to the measured HONO. As illustrated in this figure, modeled OH concentrations were approximately 80% lower than the measured values. The model also underestimates the nighttime measurements, although the measurements at night were near the detection limit of the instrument. Given that the modeled total OH reactivity is similar to measurements conducted at this site (Fig. S5), this discrepancy suggests that the model is missing a significant radical source, although the measurements may include unknown interferences.

The total radical budget resulting from the model is shown in Fig. 6. Radical initiation is largely controlled by the ozonolysis of monoterpenes during the daytime when it contributes about 70% of the total initiation. Radical initiation resulting from photolysis is relatively small with a total contribution of approximately 11%. Only about 1% of the daytime initiation results from the photolysis of HONO, suggesting HONO is not a significant source of radicals below the canopy at this site. HO_2 + RO_2 reactions dominate radical termination (47%) during the day while NO_x reactions account for approximately 36% of total radical termination. At night, the HO_2 + RO_2 reactions contribute approximately 32% while the NO_x reactions contribute 46% to radical termination.

4. Discussion

Previous studies in forested environments highlight the complexity of HONO sources and sinks, with results varying by region and season. Previous measurements at this site reported HONO mixing ratios ranging from a few ppt to 300 ppt at a minimum height of 5 m and a mean upward flux attributed to canopy emissions (Table S5).[26,83–85] Similar surface-driven production was observed in a Colorado wintertime forest study, where nocturnal HONO exceeded 1 ppb due to heterogeneous NO_2 conversion, although deposition remained a major sink.[29] By comparison, a study in Germany found that the forest floor primarily acted as a sink, with minimal soil emissions.[87] This study aligns with these previous studies, which suggest that surface processes dominate local HONO dynamics.

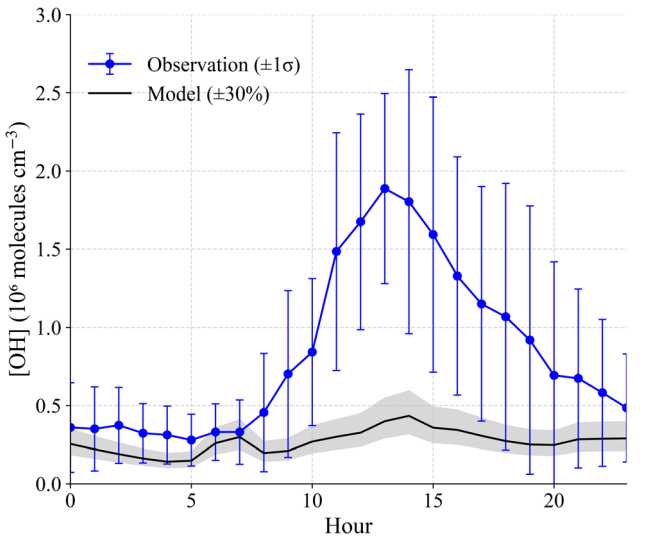

Fig. 5 Comparison between model predictions (black) and measurements (blue) of OH concentrations during the MOBCAT 2022 field campaign. Error bars represent one standard deviation of variability (±1σ). The shaded region represents estimated 30% error for the modeled OH.

4.1 Potential influence of soil emissions

Soil HONO emissions were excluded from the updated model based on a combination of environmental constraints and observational evidence. First, the average measured soil pH in the study area was approximately 6, which is significantly higher than the pK_a of HONO (3.29).[9] Under these mildly acidic conditions, thermodynamic equilibrium favors the deposition of HONO to the soil rather than its emission. Given the average soil pH at the site, the soil in this region is not expected to contribute to HONO emissions, but instead will favor HONO deposition.[88] Second, emission inventories and previous studies suggest that soil emissions of HONO and reactive nitrogen species (NO_y) are typically minimal in forested areas in the Eastern United States, particularly in undisturbed regions such as Northern Michigan.[37,89] Previous measurements of soil NO flux at this site yielded values of approximately 180 nmol m^{-2} h^{-1} which is relatively small compared to the estimated soil NO_y emissions in the eastern United States between about 535 nmol m^{-2} h^{-1} and 2220 nmol m^{-2} h^{-1}.[37,90] To estimate the potential influence of soil emissions, the previously measured NO flux (180 nmol m^{-2} h^{-1}) was used as an upper limit of HONO emissions, as HONO may be emitted at a lower rate than NO.[15,91] At this emission rate, the modeled increase in daytime HONO was relatively small (~13%) (Fig. S8). To account for the difference between the model and the measurements, an average daytime emission rate of approximately 540 nmol m^{-2} h^{-1} would be needed, with a maximum rate of about 720 nmol m^{-2} h^{-1} (Fig. S8). Taken together, these factors provide a strong basis for excluding HONO soil emissions from the model without compromising the accuracy of HONO source representation for this study area.

4.2 Impact of model uncertainties

The remaining differences between the model and observations could be accounted for by a combination of a lower HONO uptake coefficient or a higher NO_2 uptake coefficient. As described in Section 2.3, there is a wide range of acceptable uptake coefficients in the literature for HONO (10^{-4} to 10^{-6})[71,81] and NO_2 (10^{-5} to 10^{-7}).[29,92] The HONO uptake coefficient used in this study was closer to the lower end of this range (Fig. S5), suggesting the model could be improved by including a larger NO_2 uptake coefficient, which was calculated to be approximately 10^{-6}, in the middle of the reported range. However, increasing the NO_2 uptake coefficient in the model would result in an overestimation of the modeled HONO at night, when the

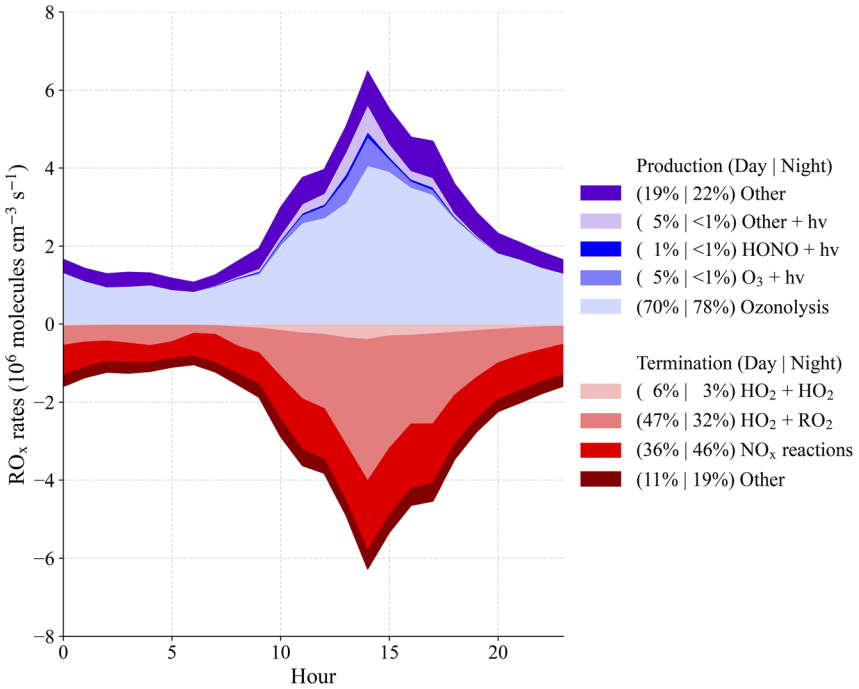

Fig. 6 Total RO_x (RO_x = OH + HO_2 + RO_2) radical budget with average daytime (08:00–20:00) and nighttime (20:00–08:00) contributions of each initiation (blue and purple) and termination (red) reaction rates.

model most closely reproduces the measurements. Another possible explanation for the daytime model underestimation of the measurements is an underestimation of the contribution of photoenhanced NO_2 hydrolysis to the production of HONO. However, the photoenhancement factor would need to be increased by two orders of magnitude in order to fully explain the measured concentrations, which is unlikely given that the photolysis rates below the canopy are approximately one order of magnitude less than that above the canopy (Fig. 2).

4.3 Influence of precipitation and meteorology on HONO sources and sinks

While the diurnal average mixing ratio of HONO was approximately 20 ppt, elevated mixing ratios of HONO were observed on several days, most notably during rain events that occurred on 1, 2, 6, and 7 August (Fig. 1). To test whether the model is able to capture the observed increase during these and other high-RH events, modeling was conducted for each of these days using photostationary state derived NO values. As discussed above, the photostationary state concentrations of NO may be lower than the actual NO mixing ratios, as a result the modeled HONO for these days are likely to be a lower limit as production from the reaction between OH and NO could be underestimated.

The model underestimated the average daytime measured HONO concentrations for these days by approximately 44% and overestimated the measured concentrations at night, although the modeled HONO agreed with the measurements to within their combined uncertainty on these days (Fig. 7a). The HONO budget for these days indicates that the modeled rate of NO_2 hydrolysis was higher compared to the campaign average and accounted for 83% of daytime HONO production and 99% at night. Similarly, deposition was dominant during the day (82%) and at night (96%), emphasizing the importance of surface interactions for both production and loss (Fig. 7b).

However, the model was unable to reproduce the measured variations during each of the rain events. On 1 August, measured mixing ratios of HONO rose from approximately 20 to 40 ppt between 08:00 and 10:00, coinciding with the onset of rain and limited solar radiation and remained elevated (Fig. 1, S9). The modeled HONO increased prior to the rain event due to an increase in NO_2 but failed to capture the elevated mixing ratios after the rain event, instead simulating a decrease in HONO driven primarily by deposition (Fig. S10). This may suggest that the model is overestimating HONO deposition post rainfall. Although soil pH was only measured during dry periods, precipitation is expected to lower pH, potentially reducing HONO uptake (E11). The morning increase in HONO may also reflect dew/fog evaporation, as temperature was relatively low and relative humidity was high overnight.[93] However, NO_2 concentrations also increased during this period, leading to enhanced NO_2 hydrolysis (Fig. S10a), making it difficult to distinguish between these two potential sources.

In contrast, HONO decreased during precipitation events on 2, 6, and 7 August (Fig. S9), likely due to wet scavenging, a process previously reported for rain, dew, and fog.[21,93,94] The overnight precipitation event from 1–2 August (23:54–07:54) ended around 08:00 when dew/fog evaporation would typically release accumulated HONO. However, HONO concentrations decreased during this period rather than showing the expected morning enhancement, inconsistent with the dew/fog evaporation hypothesis. Similarly, on 6 August, HONO decreased

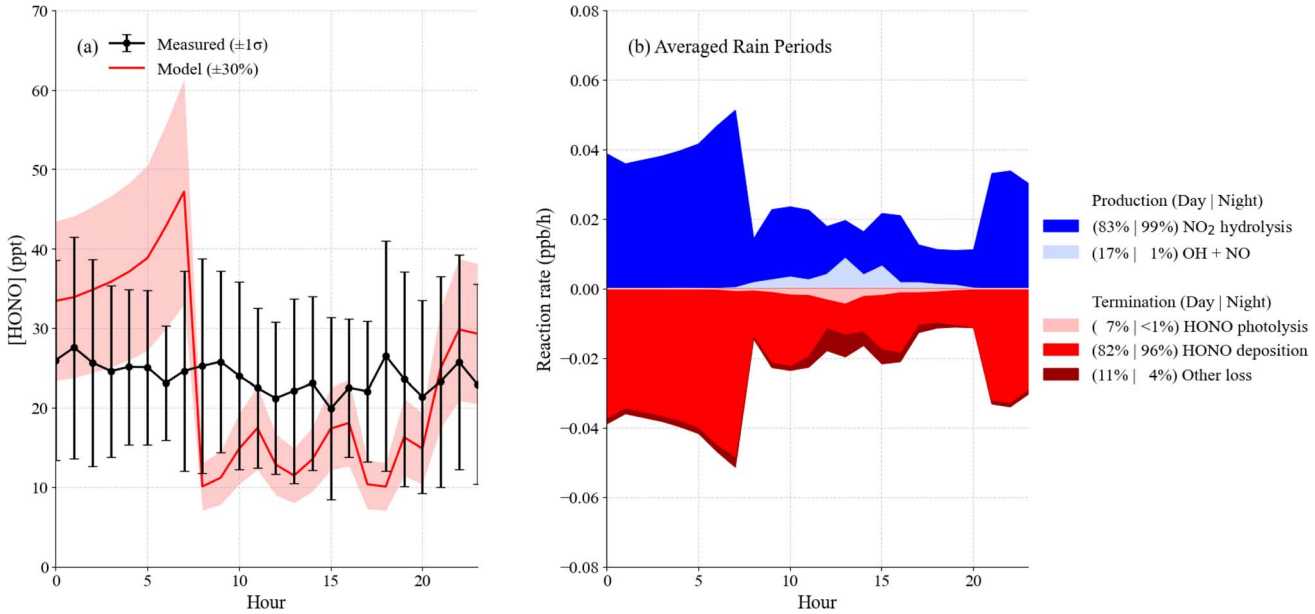

Fig. 7 Average measured (black) and modeled (red) HONO during the rain events (a) and the corresponding HONO budget (b) with stacked rates of production (blue) and loss (red).

from early morning throughout the day until the precipitation event (15:54–17:54), despite high relative humidity conditions that would favor dew/fog formation and evaporation. On 7 August, precipitation extended through much of the day (02:54–17:54), limiting typical overnight dew accumulation and morning evaporation. While a brief HONO spike occurred from 6:00–7:00 AM that could be attributed to dew/fog evaporation (Fig. S9), this peak coincided with elevated NO_2 concentrations, again preventing clear attribution to dew/fog evaporation.

Complex micrometeorological processes within and above forest canopies, including deep ventilation events, can substantially impact the distribution and dynamics of reactive trace gases. These events, driven by sudden changes in wind speed and direction, disrupt steady-state assumptions in atmospheric models and create strong vertical and temporal variability in chemical concentrations. Deep ventilation has been shown to cause large discrepancies between measured fluxes and actual surface exchange of reactive nitrogen species.[95] Observations of steep NO and NO_2 gradients and frequent failures of stationarity tests indicate intermittent mixing and chemical flux divergence, where reactions within the canopy alter species during transport so that fluxes measured aloft do not represent true emission or deposition. These episodes occur most often during morning and evening transition periods and under stable nocturnal conditions.

Similar dynamics could influence HONO measurements near the surface. While the direction and magnitude of HONO changes during ventilation events remain uncertain, enhanced mixing could redistribute HONO within and above the canopy, affecting observed concentrations at a single height. These processes may contribute to variability observed during precipitation events. Sudden bursts of turbulent mixing can transport air rapidly across canopy layers, creating conditions where HONO sources and sinks cannot be described by models that assume uniform mixing.[96] While this study lacked wind data needed to identify individual ventilation events, future work should combine turbulence measurements, eddy covariance fluxes, and vertical HONO profiles to better constrain canopy-atmosphere exchange and improve model performance.

4.4 Implications for below canopy radical production

The contribution of HONO to radical production varies in different forests. In some cases, HONO photolysis plays a minimal role in local radical budgets. At the Blodgett Forest Research Station in California, HONO contributed to approximately 6% to total radical production above the forest canopy.[97] At that site, diurnal average HONO mixing ratios ranged from 25 to 60 ppt and exhibited a clear daytime decrease, similar to trends observed here. Similarly, measurements of HONO at the Indiana University Research and Teaching Preserve forest site near Bloomington were found to contribute to less than 3% of total radical production, with mixing ratios ranging from 10–40 ppt.[49] In contrast, other studies at forested sites have found that HONO photolysis can be a major source of radical production, accounting for over 25% of the total HO_x production.[19,21,98,99] For example, measurements of HONO in a forest near Jülich, Germany were found to reach 0.5–2 ppb at night and decreased to minimum values of 40–300 ppt during the day, contributing to approximately 33% of total OH production at that site.[19]

Previous measurements above the forest canopy at the PROPHET site found that HONO was a significant source of radicals, contributing 13–17% of total radical initiation,[44,62] with maximum measured mixing ratios of HONO of greater than 50 ppt during the day due to increased production from the photolysis of nitric acid on the forest canopy surfaces.[100] The reduced photon flux below the canopy results in lower HONO

production by this mechanism and combined with the lower photolysis rates results in HONO contributing only 1% of the total radical production during the day below the forest canopy (Fig. 6).

Given the limited contribution of HONO to radical production at this site (Fig. 6), another unidentified OH source may be responsible for the discrepancy between the modeled and observed concentrations. While instrumental interferences may have contributed to the measured OH concentrations, another plausible explanation for the discrepancy is the ozonolysis of an unidentified, biogenic very reactive VOC (VRVOC). A previous study estimated OH and RO_2 production to be enhanced by up to 1 ppt s^{-1} when using β-caryophyllene as a proxy for VRVOCs and β-pinene as the VRVOC derived RO_2.[8] Under high reactivity conditions with 1 : 1 yields of OH and RO_2 from the ozonolysis of VRVOCs, the OH concentration increased relative to the base model without VRVOCs.[8] The limited measurements of terpenes and oxygenated VOCs in this study leave open the possibility that these unaccounted-for compounds are a major contributor to radical production, resulting in OH radical concentrations similar to that produced above the forest canopy and contributing to the production of oxygenated VOCs and SOA below the canopy, which could impact the concentration of these secondary pollutants above the forest canopy.[9]

5. Conclusions

Below-canopy measurements near the surface revealed maximum mixing ratios of approximately 52 ppt for HONO and approximately 3×10^6 cm^{-3} for OH radicals, with average concentrations of approximately 20 ppt and 8×10^5 cm^{-3} for HONO and OH, respectively. HONO exhibited a nighttime maximum and a daytime minimum, with below-canopy values lower than previous above-canopy measurements, likely due to reduced surface photolysis and increased deposition.[26,100] The measured OH concentrations were similar to previous above-canopy measurements at this site,[44] and higher than 1-D canopy model predictions,[6] but should be considered an upper limit due to the lack of interference testing.

A 0-D model incorporating both gas-phase and heterogeneous production and loss of HONO reproduced the average measured HONO concentrations to within the uncertainty of the measurements. Daytime production of HONO was dominated by the reaction between OH and NO, while heterogeneous conversion of NO_2 on ground surfaces dominated HONO production at night. Photolysis and surface deposition dominated the loss of HONO during the day and night, respectively. These results highlight the importance of heterogeneous production and loss processes for surface HONO, while other sources of HONO such as soil emissions appear to be negligible at this site.

Mixing ratios of HONO increased during precipitation events, suggesting that rain adds complexity to HONO sources and sinks, and the model could not reproduce the observed variations during each event. Additional measurements of HONO concentrations during rain events are needed to help refine model predictions. Reduced photolysis below the forest canopy resulted in a relatively long HONO lifetime (~45 minutes), suggesting that vertical transport of HONO may be important and therefore the 0-D model may not be appropriate. Further studies of vertical profiling and 1-D modeling are needed to further characterize HONO chemistry in forest environments.

Measured concentrations of OH were similar to previous observations above the canopy at this site, suggesting that significant chemical oxidation was occurring in the canopy that could impact the concentration of oxygenated VOCs and SOA above the canopy. Ozonolysis of monoterpenes was a dominant source of radicals below the canopy, accounting for 70% of total radical initiation during the day. Photolysis of HONO contributed to approximately 1% of total radical initiation, suggesting that at this site, HONO is not an important source of OH radicals beneath the canopy. The model underestimated the measured OH concentrations by approximately 80%, with unmeasured instrumental interferences or the ozonolysis of unmeasured reactive VOCs potentially responsible for the discrepancy. A more detailed analysis of the below canopy radical chemistry measured at this site, including measurements of peroxy radical concentrations, will be presented in a future publication.

Author contributions

BH, ER, IS, AH, and BB conducted the measurements under the guidance of PSS. BH conducted the analysis and photochemical modeling. BH and PSS wrote the paper with feedback from all co-authors.

Conflicts of interest

There are no conflicts of interest to declare.

Data availability

Data for this article, including all field campaign measurements are available at https://doi.org/10.6084/m9.figshare.28778915.

Supplementary information (SI) is available. See DOI: https://doi.org/10.1039/d5ea00122f.

Acknowledgements

This research was supported by the National Science Foundation (grants AGS-1827450 and AGS-2322462), the Indiana Space Grant Consortium (INSGC), and the University of Michigan Biological Station Marian P. and David M. Gates Graduate Student Fellowship. The authors would like to thank the UMBS staff for their assistance and logistical support, and James Flynn from the University of Houston for the use of the radiometer.

References

1 P. A. Makar, R. M. Staebler, A. Akingunola, J. Zhang, C. McLinden, S. K. Kharol, B. Pabla, P. Cheung and Q. Zheng, The effects of forest canopy shading and

turbulence on boundary layer ozone, *Nat. Commun.*, 2017, **8**, 15243.

2 A. H. Goldstein, M. McKay, M. R. Kurpius, G. W. Schade, A. Lee, R. Holzinger and R. A. Rasmussen, Forest thinning experiment confirms ozone deposition to forest canopy is dominated by reaction with biogenic VOCs, *Geophys. Res. Lett.*, 2004, **31**, L22106.

3 A. Hogg, J. Uddling, D. Ellsworth, M. A. Carroll, S. Pressley, B. Lamb and C. Vogel, Stomatal and non-stomatal fluxes of ozone to a northern mixed hardwood forest, *Tellus B*, 2007, **59**, 514–525.

4 M. R. Kurpius and A. H. Goldstein, Gas-phase chemistry dominates O_3 loss to a forest, implying a source of aerosols and hydroxyl radicals to the atmosphere, *Geophys. Res. Lett.*, 2003, **30**, 1371.

5 M. P. Vermeuel, D. B. Millet, D. K. Farmer, L. N. Ganzeveld, A. J. Visser, H. D. Alwe, T. H. Bertram, P. A. Cleary, A. R. Desai, D. Helmig, S. C. Kavassalis, M. F. Link, M. A. Pothier, M. Riches, W. Wang and S. Williams, A Vertically Resolved Canopy Improves Chemical Transport Model Predictions of Ozone Deposition to North Temperate Forests, *J. Geophys. Res.: Atmos.*, 2024, **129**, e2024JD042092.

6 A. M. Bryan, S. B. Bertman, M. A. Carroll, S. Dusanter, G. D. Edwards, R. Forkel, S. Griffith, A. B. Guenther, R. F. Hansen, D. Helmig, B. T. Jobson, F. N. Keutsch, B. L. Lefer, S. N. Pressley, P. B. Shepson, P. S. Stevens and A. L. Steiner, In-canopy gas-phase chemistry during CABINEX 2009: sensitivity of a 1-D canopy model to vertical mixing and isoprene chemistry, *Atmos. Chem. Phys.*, 2012, **12**, 8829–8849.

7 R. Holzinger, A. Lee, K. T. Paw and U. A. H. Goldstein, Observations of oxidation products above a forest imply biogenic emissions of very reactive compounds, *Atmos. Chem. Phys.*, 2005, **5**, 67–75.

8 G. M. Wolfe, J. A. Thornton, M. McKay and A. H. Goldstein, Forest-atmosphere exchange of ozone: sensitivity to very reactive biogenic VOC emissions and implications for in-canopy photochemistry, *Atmos. Chem. Phys.*, 2011, **11**, 7875–7891.

9 B. C. Schulze, H. W. Wallace, J. H. Flynn, B. L. Lefer, M. H. Erickson, B. T. Jobson, S. Dusanter, S. M. Griffith, R. F. Hansen, P. S. Stevens, T. VanReken and R. J. Griffin, Differences in BVOC oxidation and SOA formation above and below the forest canopy, *Atmos. Chem. Phys.*, 2017, **17**, 1805–1828.

10 Y. F. Elshorbany, J. Kleffmann, R. Kurtenbach, E. Lissi, M. Rubio, G. Villena, E. Gramsch, A. R. Rickard, M. J. Pilling and P. Wiesen, Seasonal dependence of the oxidation capacity of the city of Santiago de Chile, *Atmos. Environ.*, 2010, **44**, 5383–5394.

11 Z. Tan, H. Fuchs, K. Lu, A. Hofzumahaus, B. Bohn, S. Broch, H. Dong, S. Gomm, R. Häseler, L. He, F. Holland, X. Li, Y. Liu, S. Lu, F. Rohrer, M. Shao, B. Wang, M. Wang, Y. Wu, L. Zeng, Y. Zhang, A. Wahner and Y. Zhang, Radical chemistry at a rural site (Wangdu) in the North China Plain: observation and model calculations of OH, HO2 and RO2 radicals, *Atmos. Chem. Phys.*, 2017, **17**, 663–690.

12 R. Kurtenbach, K. H. Becker, J. A. G. Gomes, J. Kleffmann, J. C. Lörzer, M. Spittler, P. Wiesen, R. Ackermann, A. Geyer and U. Platt, Investigations of emissions and heterogeneous formation of HONO in a road traffic tunnel, *Atmos. Environ.*, 2001, **35**, 3385–3394.

13 H. Xuan, C. Liu, P. Zhang, B. Chu, L. Liang, Q. Ma and H. He, A Review of Laboratory Studies on the Heterogeneous Chemistry of NO_2: Mechanisms and Uptake Kinetics, *J. Phys. Chem. A*, 2025, **129**, 815–835.

14 C. Ye, N. Zhang, H. Gao and X. Zhou, Photolysis of Particulate Nitrate as a Source of HONO and NO_x, *Environ. Sci. Technol.*, 2017, **51**, 6849–6856.

15 R. Oswald, T. Behrendt, M. Ermel, D. Wu, H. Su, Y. Cheng, C. Breuninger, A. Moravek, E. Mougin, C. Delon, B. Loubet, A. Pommerening-Röser, M. Sörgel, U. Pöschl, T. Hoffmann, M. O. Andreae, F. X. Meixner and I. Trebs, HONO Emissions from Soil Bacteria as a Major Source of Atmospheric Reactive Nitrogen, *Science*, 2013, **341**, 1233–1235.

16 Y. F. Elshorbany, R. Kurtenbach, P. Wiesen, E. Lissi, M. Rubio, G. Villena, E. Gramsch, A. R. Rickard, M. J. Pilling and J. Kleffmann, Oxidation capacity of the city air of Santiago, Chile, *Atmos. Chem. Phys.*, 2009, **9**, 2257–2273.

17 B. J. Finlayson-Pitts and J. N. Pitts, *Chemistry of the Upper and Lower Atmosphere: Theory, Experiments, and Applications*, Academic Press, 2000.

18 J. B. Burkholder, S. P. Sander, J. P. D. Abbatt, J. R. Barker and C. Cappa, *JPL Publication 19-5. Chemical Kinetics and Photochemical Data for Use in Atmospheric Studies*, Jet Propulsion Laboratory, 2019.

19 J. Kleffmann, T. Gavriloaiei, A. Hofzumahaus, F. Holland, R. Koppmann, L. Rupp, E. Schlosser, M. Siese and A. Wahner, Daytime formation of nitrous acid: A major source of OH radicals in a forest, *Geophys. Res. Lett.*, 2005, **32**, L05818.

20 M. Sörgel, E. Regelin, H. Bozem, J. M. Diesch, F. Drewnick, H. Fischer, H. Harder, A. Held, Z. Hosaynali-Beygi, M. Martinez and C. Zetzsch, Quantification of the unknown HONO daytime source and its relation to NO_2, *Atmos. Chem. Phys.*, 2011, **11**, 10433–10447.

21 X. Zhou, K. Civerolo, H. Dai, G. Huang, J. Schwab and K. Demerjian, Summertime nitrous acid chemistry in the atmospheric boundary layer at a rural site in New York State, *J. Geophys. Res.: Atmos.*, 2002, **107**, 4590.

22 R. M. Harrison and A.-M. N. Kitto, Evidence for a surface source of atmospheric nitrous acid, *Atmos. Environ.*, 1994, **28**, 1089–1094.

23 J. Kleffmann, Daytime Sources of Nitrous Acid (HONO) in the Atmospheric Boundary Layer, *ChemPhysChem*, 2007, **8**, 1137–1144.

24 K. Stemmler, M. Ammann, C. Donders, J. Kleffmann and C. George, Photosensitized reduction of nitrogen dioxide on humic acid as a source of nitrous acid, *Nature*, 2006, **440**, 195–198.

25 K. Stemmler, M. Ndour, Y. Elshorbany, J. Kleffmann, B. D'Anna, C. George, B. Bohn and M. Ammann, Light induced conversion of nitrogen dioxide into nitrous acid on sub micron humic acid aerosol, *Atmos. Chem. Phys.*, 2007, **7**, 4237–4248.

26 N. Zhang, X. Zhou, S. Bertman, D. Tang, M. Alaghmand, P. B. Shepson and M. A. Carroll, Measurements of ambient HONO concentrations and vertical HONO flux above a northern Michigan forest canopy, *Atmos. Chem. Phys.*, 2012, **12**, 8285–8296.

27 P. S. Romer, P. J. Wooldridge, J. D. Crounse, M. J. Kim, P. O. Wennberg, J. E. Dibb, E. Scheuer, D. R. Blake, S. Meinardi, A. L. Brosius, A. B. Thames, D. O. Miller, W. H. Brune, S. R. Hall, T. B. Ryerson and R. C. Cohen, Constraints on Aerosol Nitrate Photolysis as a Potential Source of HONO and NO_x, *Environ. Sci. Technol.*, 2018, **52**, 13738–13746.

28 Y. Song, Y. Zhang, C. Xue, P. Liu, X. He, X. Li and Y. Mu, The seasonal variations and potential sources of nitrous acid (HONO) in the rural North China Plain, *Environ. Pollut.*, 2022, **311**, 119967.

29 T. C. VandenBoer, S. S. Brown, J. G. Murphy, W. C. Keene, C. J. Young, A. A. P. Pszenny, S. Kim, C. Warneke, J. A. Gouw, J. R. Maben, N. L. Wagner, T. P. Riedel, J. A. Thornton, D. E. Wolfe, W. P. Dubé, F. Öztürk, C. A. Brock, N. Grossberg, B. Lefer, B. Lerner, A. M. Middlebrook and J. M. Roberts, Understanding the role of the ground surface in HONO vertical structure: High resolution vertical profiles during NACHTT-11, *J. Geophys. Res.: Atmos.*, 2013, **118**(10), 155–171.

30 A. Geyer and J. Stutz, Vertical profiles of NO_3, N_2O_5, O_3, and NO_x in the nocturnal boundary layer: 2. Model studies on the altitude dependence of composition and chemistry, *J. Geophys. Res.: Atmos.*, 2004, **109**, D12307.

31 K. W. Wong, C. Tsai, B. Lefer, C. Haman, N. Grossberg, W. H. Brune, X. Ren, W. Luke and J. Stutz, Daytime HONO vertical gradients during SHARP 2009 in Houston, TX, *Atmos. Chem. Phys.*, 2012, **12**, 635–652.

32 H. Su, Y. Cheng, R. Oswald, T. Behrendt, I. Trebs, F. X. Meixner, M. O. Andreae, P. Cheng, Y. Zhang and U. Pöschl, Soil Nitrite as a Source of Atmospheric HONO and OH Radicals, *Science*, 2011, **333**, 1616–1618.

33 M. Ermel, T. Behrendt, R. Oswald, B. Derstroff, D. Wu, S. Hohlmann, C. Stönner, A. Pommerening-Röser, M. Könneke, J. Williams, F. X. Meixner, M. O. Andreae, I. Trebs and M. Sörgel, Hydroxylamine released by nitrifying microorganisms is a precursor for HONO emission from drying soils, *Sci. Rep.*, 2018, **8**, 1877.

34 K. Tang, M. Qin, B. Han, D. Shao, Z. Xu, H. Sun and Y. Wu, Identifying the influencing factors of soil nitrous acid emissions using random forest model, *Atmos. Environ.*, 2024, **339**, 120875.

35 B. Weber, D. Wu, A. Tamm, N. Ruckteschler, E. Rodríguez-Caballero, J. Steinkamp, H. Meusel, W. Elbert, T. Behrendt, M. Sörgel, Y. Cheng, P. J. Crutzen, H. Su and U. Pöschl, Biological soil crusts accelerate the nitrogen cycle through large NO and HONO emissions in drylands, *Proc. Natl. Acad. Sci. U. S. A.*, 2015, **112**, 15384–15389.

36 D. Wu, M. A. Horn, T. Behrendt, S. Müller, J. Li, J. A. Cole, B. Xie, X. Ju, G. Li, M. Ermel, R. Oswald, J. Fröhlich-Nowoisky, P. Hoor, C. Hu, M. Liu, M. O. Andreae, U. Pöschl, Y. Cheng, H. Su, I. Trebs, B. Weber and M. Sörgel, Soil HONO emissions at high moisture content are driven by microbial nitrate reduction to nitrite: tackling the HONO puzzle, *ISME J.*, 2019, **13**, 1688–1699.

37 R. M. Mushinski, R. P. Phillips, Z. C. Payne, R. B. Abney, I. Jo, S. Fei, S. E. Pusede, J. R. White, D. B. Rusch and J. D. Raff, Microbial mechanisms and ecosystem flux estimation for aerobic NO_y emissions from deciduous forest soils, *Proc. Natl. Acad. Sci. U. S. A.*, 2019, **116**, 2138–2145.

38 C. Xue, C. Ye, C. Zhang, V. Catoire, P. Liu, R. Gu, J. Zhang, Z. Ma, X. Zhao, W. Zhang, Y. Ren, G. Krysztofiak, S. Tong, L. Xue, J. An, M. Ge, A. Mellouki and Y. Mu, Evidence for Strong HONO Emission from Fertilized Agricultural Fields and its Remarkable Impact on Regional O_3 Pollution in the Summer North China Plain, *ACS Earth Space Chem.*, 2021, **5**, 340–347.

39 Y. Wang, X. Fu, D. Wu, M. Wang, K. Lu, Y. Mu, Z. Liu, Y. Zhang and T. Wang, Agricultural fertilization aggravates air pollution by stimulating soil nitrous acid emissions at high soil moisture, *Environ. Sci. Technol.*, 2021, **55**, 14556.

40 D. Wu, J. Zhang, M. Wang, J. An, R. Wang, H. Haider, X. Ri, Y. Huang, Q. Zhang, F. Zhou, H. Tian, X. Zhang, L. Deng, Y. Pan, X. Chen, Y. Yu, C. Hu, R. Wang, Y. Song, Z. Gao, Y. Wang, L. Hou and M. Liu, Global and regional patterns of soil nitrous acid emissions and their acceleration of rural photochemical reactions, *J. Geophys. Res.: Atmos.*, 2022, **127**, e2021JD036379.

41 D. Tan, I. Faloona, J. B. Simpas, W. Brune, P. B. Shepson, T. L. Couch, A. L. Sumner, M. A. Carroll, T. Thornberry, E. Apel, D. Riemer and W. Stockwell, HO_x budgets in a deciduous forest: Results from the PROPHET summer 1998 campaign, *J. Geophys. Res.: Atmos.*, 2001, **106**, 24407–24427.

42 M. A. Carroll, S. B. Bertman and P. B. Shepson, Overview of the Program for Research on Oxidants: PHotochemistry, Emissions, and Transport (PROPHET) summer 1998 measurements intensive, *J. Geophys. Res.: Atmos.*, 2001, **106**, 24275–24288.

43 O. R. Cooper, J. L. Moody, T. D. Thornberry, M. S. Town and M. A. Carroll, PROPHET 1998 meteorological overview and air-mass classification, *J. Geophys. Res.: Atmos.*, 2001, **106**, 24289–24299.

44 B. Bottorff, M. M. Lew, Y. Woo, P. Rickly, M. D. Rollings, B. Deming, D. C. Anderson, E. Wood, H. D. Alwe, D. B. Millet, A. Weinheimer, G. Tyndall, J. Ortega, S. Dusanter, T. Leonardis, J. Flynn, M. Erickson, S. Alvarez, J. C. Rivera-Rios, J. D. Shutter, F. Keutsch, D. Helmig, W. Wang, H. M. Allen, J. H. Slade, P. B. Shepson, S. Bertman and P. S. Stevens, OH, HO_2, and RO_2 radical chemistry in a rural forest environment:

measurements, model comparisons, and evidence of a missing radical sink, *Atmos. Chem. Phys.*, 2023, **23**, 10287–10311.

45 B. Seok, D. Helmig, L. Ganzeveld, M. W. Williams and C. S. Vogel, Dynamics of nitrogen oxides and ozone above and within a mixed hardwood forest in northern Michigan, *Atmos. Chem. Phys.*, 2013, **13**, 7301–7320.

46 D. L. Sparks, A. L. Page, P. A. Helmke and R. H. Loeppert, in *Methods of Soil Analysis*, John Wiley & Sons, 2020, p. 1424.

47 B. Bottorff, E. Reidy, L. Mielke, S. Dusanter and P. S. Stevens, Development of a laser-photofragmentation laser-induced fluorescence instrument for the detection of nitrous acid and hydroxyl radicals in the atmosphere, *Atmos. Meas. Tech.*, 2021, **14**, 6039–6056.

48 S. Dusanter, D. Vimal and P. S. Stevens, Technical note: Measuring tropospheric OH and HO_2 by laser- induced fluorescence at low pressure. A comparison of calibration techniques, *Atmos. Chem. Phys.*, 2008, **8**, 321–340.

49 M. Lew, P. Rickly, B. Bottorff, E. Reidy, S. Sklaveniti, T. Léonardis, N. Locoge, S. Dusanter, S. Kundu, E. Wood and P. S. Stevens, OH and HO_2 radical chemistry in a midlatitude forest: measurements and model comparisons, *Atmos. Chem. Phys.*, 2020, **20**, 9209–9230.

50 P. Rickly and P. S. Stevens, Measurements of a potential interference with laser-induced fluorescence measurements of ambient OH from the ozonolysis of biogenic alkenes, *Atmos. Meas. Tech.*, 2018, **11**, 1–16.

51 S. M. Saunders, M. E. Jenkin, R. G. Derwent and M. J. Pilling, Protocol for the development of the Master Chemical Mechanism, MCM v3 (Part A): tropospheric degradation of non-aromatic volatile organic compounds, *Atmos. Chem. Phys.*, 2003, **3**, 161–180.

52 M. E. Jenkin, S. M. Saunders, V. Wagner and M. J. Pilling, Protocol for the development of the Master Chemical Mechanism, MCM v3 (Part B): tropospheric degradation of aromatic volatile organic compounds, *Atmos. Chem. Phys.*, 2003, **3**, 181–193.

53 M. E. Jenkin, J. C. Young and A. R. Rickard, The MCM v3.3.1 degradation scheme for isoprene, *Atmos. Chem. Phys.*, 2015, **15**, 11433–11459.

54 J. D. Crounse, F. Paulot, H. G. Kjaergaard and P. O. Wennberg, Peroxy radical isomerization in the oxidation of isoprene, *Phys. Chem. Chem. Phys.*, 2011, **13**, 13607–13613.

55 G. M. Wolfe, M. R. Marvin, S. J. Roberts, K. R. Travis and J. Liao, The Framework for 0-D Atmospheric Modeling (F0AM) v3.1, *Geosci. Model Dev.*, 2016, **9**, 3309–3319.

56 Y. Liu, K. Lu, X. Li, H. Dong, Z. Tan, H. Wang, Q. Zou, Y. Wu, L. Zeng, M. Hu, K.-E. Min, S. Kecorius, A. Wiedensohler and Y. Zhang, A Comprehensive Model Test of the HONO Sources Constrained to Field Measurements at Rural North China Plain, *Environ. Sci. Technol.*, 2019, **53**, 3517–3525.

57 J. Liu, Z. Liu, Z. Ma, S. Yang, D. Yao, S. Zhao, B. Hu, G. Tang, J. Sun, M. Cheng, Z. Xu and Y. Wang, Detailed budget analysis of HONO in Beijing, China: Implication on atmosphere oxidation capacity in polluted megacity, *Atmos. Environ.*, 2021, **244**, 117957.

58 H. Hellén, A. P. Praplan, T. Tykkä, I. Ylivinkka, V. Vakkari, J. Bäck, T. Petäjä, M. Kulmala and H. Hakola, Long-term measurements of volatile organic compounds highlight the importance of sesquiterpenes for the atmospheric chemistry of a boreal forest, *Atmos. Chem. Phys.*, 2018, **18**, 13839–13863.

59 M. B. Dillon, M. S. Lamanna, G. W. Schade, A. H. Goldstein and R. C. Cohen, Chemical evolution of the Sacramento urban plume: Transport and oxidation, *J. Geophys. Res.: Atmos.*, 2002, **107**(D5), DOI: 10.1029/2001JD000969.

60 M. E. Jenkin, S. M. Saunders and M. J. Pilling, The tropospheric degradation of volatile organic compounds: a protocol for mechanism development, *Atmos. Environ.*, 1997, **31**, 81–104.

61 S. Madronich and S. Flocke, in *Environmental Photochemistry*, ed. P. Boule, Springer, Berlin, Heidelberg, 1999, pp. 1–26, DOI: 10.1007/978-3-540-69044-3_1.

62 S. M. Griffith, R. F. Hansen, S. Dusanter, P. S. Stevens, M. Alaghmand, S. B. Bertman, M. A. Carroll, M. Erickson, M. Galloway, N. Grossberg, J. Hottle, J. Hou, B. T. Jobson, A. Kammrath, F. N. Keutsch, B. L. Lefer, L. H. Mielke, A. O'Brien, P. B. Shepson, M. Thurlow, W. Wallace, N. Zhang and X. L. Zhou, OH and HO_2 radical chemistry during PROPHET 2008 and CABINEX 2009 Part 1: Measurements and model comparison, *Atmos. Chem. Phys.*, 2013, **13**, 5403–5423.

63 C. Ye, X. Zhou, D. Pu, J. Stutz, J. Festa, M. Spolaor, C. Cantrell, R. L. Mauldin, A. Weinheimer and J. Haggerty, Comment on "Missing gas-phase source of HONO inferred from Zeppelin measurements in the troposphere", *Science*, 2015, **348**, 1326.

64 J. D. Lee, L. K. Whalley, D. E. Heard, D. Stone, R. E. Dunmore, J. F. Hamilton, D. E. Young, J. D. Allan, S. Laufs and J. Kleffmann, Detailed budget analysis of HONO in central London reveals a missing daytime source, *Atmos. Chem. Phys.*, 2016, **16**, 2747–2764.

65 I. Bejan, Y. A. E. Aal, I. Barnes, T. Benter, B. Bohn, P. Wiesen and J. Kleffmann, The photolysis of ortho-nitrophenols: a new gas phase source of HONO, *Phys. Chem. Chem. Phys.*, 2006, **8**, 2028–2035.

66 W. H. Chan, R. J. Nordstrom, J. G. Calvert and J. H. Shaw, Kinetic study of nitrous acid formation and decay reactions in gaseous mixtures of nitrous acid, nitrogen oxide (NO), nitrogen oxide (NO_2), water, and nitrogen, *Environ. Sci. Technol.*, 1976, **10**, 674–682.

67 W. Liao, A. Hecobian, J. Mastromarino and D. Tan, Development of a photo-fragmentation/laser-induced fluorescence measurement of atmospheric nitrous acid, *Atmos. Environ.*, 2006, **40**, 17–26.

68 C. Xue, C. Zhang, C. Ye, P. Liu, V. Catoire, G. Krysztofiak, H. Chen, Y. Ren, X. Zhao, J. Wang, F. Zhang, C. Zhang, J. Zhang, J. An, T. Wang, J. Chen, J. Kleffmann, A. Mellouki and Y. Mu, HONO Budget and Its Role in Nitrate Formation in the Rural North China Plain, *Environ. Sci. Technol.*, 2020, **54**, 11048–11057.

69 L. Zhang, T. Wang, Q. Zhang, J. Zheng, Z. Xu and M. Lv, Potential sources of nitrous acid (HONO) and their impacts on ozone: A WRF-Chem study in a polluted subtropical region, *J. Geophys. Res.: Atmos.*, 2016, **121**, 3645–3662.

70 M. A. Donaldson, A. E. Berke and J. D. Raff, Uptake of Gas Phase Nitrous Acid onto Boundary Layer Soil Surfaces, *Environ. Sci. Technol.*, 2014, **48**, 375–383.

71 M. A. Donaldson, D. L. Bish and J. D. Raff, Soil surface acidity plays a determining role in the atmospheric terrestrial exchange of nitrous acid, *Proc. Natl. Acad. Sci. U. S. A.*, 2014, **111**, 18472–18477.

72 A. El Zein, M. N. Romanias and Y. Bedjanian, Kinetics and Products of Heterogeneous Reaction of HONO with Fe_2O_3 and Arizona Test Dust, *Environ. Sci. Technol.*, 2013, **47**, 6325–6331.

73 M. N. Romanias, A. El Zein and Y. Bedjanian, Reactive uptake of HONO on aluminium oxide surface, *J. Photochem. Photobiol. Chem.*, 2012, **250**, 50–57.

74 K. W. Wong and J. Stutz, Influence of nocturnal vertical stability on daytime chemistry: A one-dimensional model study, *Atmos. Environ.*, 2010, **44**, 3753–3760.

75 B. Hu, J. Duan, Y. Hong, L. Xu, M. Li, Y. Bian, M. Qin, W. Fang, P. Xie and J. Chen, Exploration of the atmospheric chemistry of nitrous acid in a coastal city of southeastern China: results from measurements across four seasons, *Atmos. Chem. Phys.*, 2022, **22**, 371–393.

76 Y. Yu, P. Cheng, H. Li, W. Yang, B. Han, W. Song, W. Hu, X. Wang, B. Yuan, M. Shao, Z. Huang, Z. Li, J. Zheng, H. Wang and X. Yu, Budget of nitrous acid (HONO) at an urban site in the fall season of Guangzhou, China, *Atmos. Chem. Phys.*, 2022, **22**, 8951–8971.

77 D. Li, L. Xue, L. Wen, X. Wang, T. Chen, A. Mellouki, J. Chen and W. Wang, Characteristics and sources of nitrous acid in an urban atmosphere of northern China: Results from 1-yr continuous observations, *Atmos. Environ.*, 2018, **182**, 296–306.

78 Y. Liu, Y. Zhang, C. Lian, C. Yan, Z. Feng, F. Zheng, X. Fan, Y. Chen, W. Wang, B. Chu, Y. Wang, J. Cai, W. Du, K. R. Daellenbach, J. Kangasluoma, F. Bianchi, J. Kujansuu, T. Petäjä, X. Wang, B. Hu, Y. Wang, M. Ge, H. He and M. Kulmala, The promotion effect of nitrous acid on aerosol formation in wintertime in Beijing: the possible contribution of traffic-related emissions, *Atmos. Chem. Phys.*, 2020, **20**, 13023–13040.

79 H. Su, Y. F. Cheng, M. Shao, D. F. Gao, Z. Y. Yu, L. M. Zeng, J. Slanina, Y. H. Zhang and A. Wiedensohler, Nitrous acid (HONO) and its daytime sources at a rural site during the 2004 PRIDE-PRD experiment in China, *J. Geophys. Res.: Atmos.*, 2008, **113**, D14312.

80 A. El Zein and Y. Bedjanian, Reactive Uptake of HONO to TiO_2 Surface: "Dark" Reaction, *J. Phys. Chem. A*, 2012, **116**, 3665–3672.

81 M. N. Romanias, A. El Zein and Y. Bedjanian, Reactive uptake of HONO on aluminium oxide surface, *J. Photochem. Photobiol., A*, 2012, **250**, 50–57.

82 Y. Tang, J. An, Y. Li and F. Wang, Uncertainty in the uptake coefficient for HONO formation on soot and its impacts on concentrations of major chemical components in the Beijing–Tianjin–Hebei region, *Atmos. Environ.*, 2014, **84**, 163–171.

83 T. Thornberry, M. A. Carroll, G. J. Keeler, S. Sillman, S. B. Bertman, M. R. Pippin, K. Ostling, J. W. Grossenbacher, P. B. Shepson, O. R. Cooper, J. L. Moody and W. R. Stockwell, Observations of reactive oxidized nitrogen and speciation of NO_y during the PROPHET summer 1998 intensive, *J. Geophys. Res.: Atmos.*, 2001, **106**, 24359–24386.

84 X. Zhou, Y. He, G. Huang, T. D. Thornberry, M. A. Carroll and S. B. Bertman, Photochemical production of nitrous acid on glass sample manifold surface, *Geophys. Res. Lett.*, 2002, **29**(14), DOI: 10.1029/2002GL015080.

85 N. Zhang, X. Zhou, P. B. Shepson, H. Gao, M. Alaghmand and B. Stirm, Aircraft measurement of HONO vertical profiles over a forested region, *Geophys. Res. Lett.*, 2009, **36**, L15820, DOI: 10.11029/12009GL038999.

86 G. R. Wentworth, J. G. Murphy, K. B. Benedict, E. J. Bangs and J. L. Collett Jr, The role of dew as a night-time reservoir and morning source for atmospheric ammonia, *Atmos. Chem. Phys.*, 2016, **16**, 7435–7449.

87 M. Sörgel, I. Trebs, D. Wu and A. Held, A comparison of measured HONO uptake and release with calculated source strengths in a heterogeneous forest environment, *Atmos. Chem. Phys.*, 2015, **15**, 9237–9251.

88 X. Ren, J. E. Sanders, A. Rajendran, R. J. Weber, A. H. Goldstein, S. E. Pusede, E. C. Browne, K. E. Min and R. C. Cohen, A relaxed eddy accumulation system for measuring vertical fluxes of nitrous acid, *Atmos. Meas. Tech.*, 2011, **4**, 2093–2103.

89 C. Granier, S. Darras, H. Denier van der Gon, J. Doubalova, N. Elguindi, B. Galle, M. Gauss, M. Guevara, J.-P. Jalkanen, J. Kuenen, C. Liousse, B. Quack, D. Simpson and K. Sindelarova, *Global Emission Inventories*, DOI: 10.24381/1d158bec.

90 M. Alaghmand, P. B. Shepson, T. K. Starn, B. T. Jobson, H. W. Wallace, M. A. Carroll, S. B. Bertman, B. Lamb, S. L. Edburg, X. Zhou, E. Apel, D. Riemer, P. Stevens and F. Keutsch, The Morning NO_x maximum in the forest atmosphere boundary layer, *Atmos. Chem. Phys. Discuss.*, 2011, **11**, 29251–29282.

91 B. Cheng, Z. Han, Z. Tian, W. Liu, J. Yang, X. Gu, H. Yu, H. Wang and M. Zhou, Soil emissions of HONO and other nitrogen-containing gases: Insights into microbial pathways and moisture effects, *Atmos. Poll. Res.*, 2025, **16**, 102501.

92 J. Kleffmann, K. H. Becker and P. Wiesen, Heterogeneous NO_2 conversion processes on acid surfaces: possible atmospheric implications, *Atmos. Environ.*, 1998, **32**, 2721–2729.

93 Y. Ren, B. Stieger, G. Spindler, B. Grosselin, A. Mellouki, T. Tuch, A. Wiedensohler and H. Herrmann, Role of the dew water on the ground surface in HONO distribution:

a case measurement in Melpitz, *Atmos. Chem. Phys.*, 2020, **20**, 13069–13089.

94 M. A. Rubio, E. Lissi, G. Villena, Y. F. Elshorbany, J. Kleffmann, R. Kurtenbach and P. Wiesen, Simultaneous measurements of formaldehyde and nitrous acid in dews and gas phase in the atmosphere of Santiago, Chile, *Atmos. Environ.*, 2009, **43**, 6106–6109.

95 J. A. Geddes and J. G. Murphy, Observations of reactive nitrogen oxide fluxes by eddy covariance above two midlatitude North American mixed hardwood forests, *Atmos. Chem. Phys.*, 2014, **14**, 2939–2957.

96 S. C. Kavassalis, *PhD Thesis*, University of Toronto, 2021.

97 X. Ren, H. Gao, X. Zhou, J. D. Crounse, P. O. Wennberg, E. C. Browne, B. W. LaFranchi, R. C. Cohen, M. McKay, A. H. Goldstein and J. Mao, Measurement of atmospheric nitrous acid at Bodgett Forest during BEARPEX2007, *Atmos. Chem. Phys.*, 2010, **10**, 6283–6294.

98 K. Acker, A. Febo, S. Trick, C. Perrino, P. Bruno, P. Wiesen, D. Möller, W. Wieprecht, R. Auel, M. Giusto, A. Geyer, U. Platt and I. Allegrini, Nitrous acid in the urban area of Rome, *Atmos. Environ.*, 2006, **40**, 3123–3133.

99 X. Ren, W. H. Brune, A. Oliger, A. R. Metcalf, J. B. Simpas, T. Shirley, J. J. Schwab, C. Bai, U. Roychowdhury, Y. Li, C. Cai, K. L. Demerjian, Y. He, X. Zhou, H. Gao and J. Hou, OH, HO_2, and OH reactivity during the PMTACS–NY Whiteface Mountain 2002 campaign: Observations and model comparison, *J. Geophys. Res.: Atmos.*, 2006, **111**, D10S03.

100 X. Zhou, N. Zhang, M. TerAvest, D. Tang, J. Hou, S. Bertman, M. Alaghmand, P. B. Shepson, M. A. Carroll, S. Griffith, S. Dusanter and P. S. Stevens, Nitric acid photolysis on forest canopy surface as a source for tropospheric nitrous acid, *Nat. Geosci.*, 2011, **4**, 440–443.